Non-Darcyeffect on non-Newtonian Bingham fluid with heat transfer between two parallel plates

W. Abbas[1], Hazem Ali Attia[2], Mostafa A. M. Abdeen[3*]

[1]Basic and Applied Science Department, College of Engineering and Technology, Arab Academy for Science, Technology, and Maritime Transport,Cairo, Egypt

[2]Department of Engineering Mathematics and Physics, Faculty of Engineering, El-Fayoum University, El-Fayoum-63514, Egypt

[3]Department of Engineering Mathematics and Physics, Faculty of Engineering, Cairo University, Giza-12211, Egypt

The non-Darcy model for the Bingham fluid has a wide range of applications in energy systems and magnetic material processing. This work investigated the effect of unsteady non-Darcy flow on the velocity and temperature distributions for non-Newtonian Bingham fluid between two infinite parallel porous plates with heat transfer considering the Hall Effect. A constant pressure gradient is applied in the main axial direction and an external uniform magnetic field and uniform suction and injection are applied in the direction perpendicular to the plates. The dimensionless governing coupled momentum and energy equations taking the Joule and viscous dissipations into consideration are derived and solved numerically using the finite difference approach. The effect of porosity of the medium, Hartmann, and Hall current parameters on the velocity and temperature distributions with a Reynolds number fixed at 10 (For$R_e \geq 10$, non-Darcy model is sufficient) is investigated. It is found that the porosity and inertial effects have a marked effect on decreasing the velocity distribution in an inverse proportionality manner. Furthermore, increasing the non-Darcian parameter decreases the temperature values for each value of the porosity.

Keywords: Non-Newtonian fluid, Bingham model, Non-Darcyflow, Heat transfer, Hall current.

INTRODUCTION

Recently, Researchers have considerable interest in the study of flow phenomenon between two parallel plates because of its possible applications in many branches of science and technology, as its occurrence in rheumatic experiments to determine the constitutive properties of the fluid, in lubrication engineering, and in transportation and processing encountered in chemical engineering, etc. [1]. On the other hand, Couette flow of an electrically conducting viscous incompressible fluid under the action of a transverse magnetic field has many applications in magneto-hydrodynamic (MHD) power generators, aerodynamics heating, pumps, polymer technology, petroleum industry, and fluid droplets-sprays [2]. Bharali and Borkakati [3], studied the effect of Hall currents on magneto hydrodynamic (MHD) flow of an incompressible viscous electrically conducting fluid between two non-conducting porous plates in the presence of a strong uniform magnetic field. The steady flow of an electrically conducting, viscous, incompressible fluid bounded by two parallel infinite insulated horizontal plates and the heat transfer was studied

by Attia and Kotb [4]. Joaquín et al. [5], studied numerically the variations with velocity of suction, hall effect, Reynolds and Hartmann number, particle concentration and Eckert number on the unsteady MHD Couette Flow and heat transfer of a dusty and electrically conducting fluid between parallel plates in the presence of an external uniform magnetic field and uniform suction and injection. The transient hydromagnetic flow through a porous medium between two infinite parallel porous plates with heat transfer considering the Hall effect and the temperature dependent physical properties under constant pressure gradient was studied by Attia et al. [6]. Also, other research work concerning the flow between two parallel plates has been obtained under different physical effects [7-12].

A non-Newtonian fluid is a fluid that does not obey Newton's law of viscosity (viscosity is variable based on applied stress or force). The non-Newtonian fluid is a classical problem that has many industrial applications such as cement, drilling mud, sludge, grease, granular suspensions, aqueous foams, slurries, paints, food products, plastics and paper pulp exhibit a yield stress τ_o to allow for the motion of the fluid. Many non-Newtonian fluids, encountered in chemical engineering processes, are known to follow the so-

* To whom all correspondence should be sent:
E-mail: *mostafa_a_m_abdeen@hotmail.com*

called "Bingham model" which have a linear shear stress/shear strain relationship and require a finite yield stress before they begin to flow (the plot of shear stress against shear strain does not pass through the origin). Several examples are clay suspensions, drilling mud, toothpaste, mayonnaise, chocolate and mustard. Many authors have studied the flow of a Bingham fluid under different physical effects and geometries, Walton and Bittleston [13], described analytical and numerical solutions for the flow of a Bingham plastic in an eccentric annulus. The magneto-hydrodynamic unsteady flow of an electrically conducting viscous incompressible non-Newtonian Bingham fluid bounded by two parallel non-conducting porous plates was studied with heat transfer considering the Hall effect by Yang and Zuh [14]. Rees and Bassom [15], presented an unsteady free convection flow of a Bingham fluid when it saturates a porous medium and the flows was induced by suddenly raising the constant temperature of a vertical bounding surface.

Fluid flow in porous media is important in many areas of reservoir engineering, such as petroleum, environmental and ground water hydrology[16]. According to previous work, Darcy's law depicts fluid flow behavior in porous media. The Darcy law is sufficient in studying small rate flows where the Reynolds number is very small ($R_e < 10$) [17]. For larger Reynolds numbers the Darcy law is insufficient and several models have been adopted to correct the Darcy law. Based on a review of previous work, the Darcy-Forchheimer model is probably the most popular modification to Darcy flows. In 1901, Philippe Forchheimer assumed that Darcy's law is still valid, but an additional term must be added to account for the increased pressure drop and represent the microscopic inertial effect [18]. Recent contributions are the interesting studies considered in the references [19-24].

In the present paper, an extension has been made to the study in [25], to assess the influence of Non-Darcy porous media on unsteady non-Newtonian Bingham fluid between two infinite horizontal porous plates, by heat transfer and the Hall Effect. The fluid is acted upon by a constant pressure gradient, a uniform suction from above and a uniform injection from below while it is subjected to a uniform magnetic field perpendicular to the plates. The inclusion of the porosity effect and inertial effects as well as the velocity of suction or injection leads to some interesting effects, on both the velocity and temperature distributions to be investigated.

MATHEMATICAL MODEL

In the present model, two infinite horizontal plates located at the y = ±h planes and extended from x = 0 to ∞ and from z = 0 to ∞ have been considered and filled with incompressible, non-Newtonian fluid obeying the Bingham model and electrically conducting fluid through a porous medium. The characteristics of the porous medium in this study obey the Darcy-Forchheimer model. The fluid flows between the two plates under the influence of a pressure gradient dp/dx in the x-direction which is constant with time. The two plates are porous, insulated and kept at two constant but different temperatures T_1 for the lower plate and T_2 for the upper plate ($T_2 > T_1$). The upper plate moves with a uniform velocity U_o whereas the lower plate is kept stationary. A uniform suction from above and injection from below, with velocity v_o, are applied impulsively at $t = 0$. A uniform magnetic field $B = (0, B_o, 0)$ is applied parallel to the y-axis which is normal to the planes of the plates in the positive direction.The effect of the Hall current is considered which results in a new component for the velocity in the z-direction.
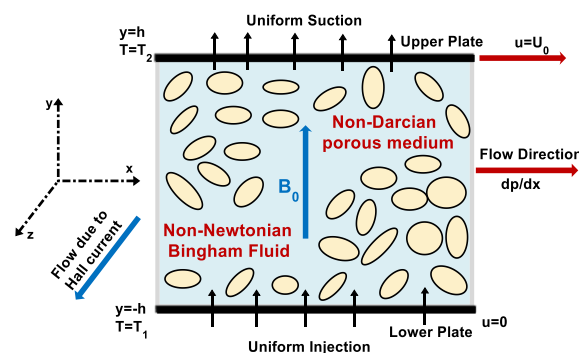

Fig. 1. Schematic diagram of the problem

From the geometry of the problem and due to the infinite dimensions in the x and z directions, it is evident that the physical quantities do not change in these directions ($\partial/\partial x = \partial/\partial z = 0$ for all quantities). The flow in the porous medium deals with the analysis in which the differential equation governing the fluid motion is based on the Darcy-Forchheimer law which considers the drag exerted by the porous medium. The fluid motion starts from rest at $t = 0$, and the no-slip condition at the plates implies that the fluid velocity has neither a z nor an x-component at $y = \pm h$. The initial temperature of the fluid is assumed to be equal to T_1 as the temperature of the lower plate. Figure 1 represents a schematic diagram of the proposed problem.

The governing equations of this study are based on the conservation laws of mass, linear momentum and energy for both phases.

The generalized Ohm's law including the Hall current is given in the form [26]:

$$\vec{J} = \sigma\left[\vec{E} + \vec{v} \times \vec{B} - \frac{1}{en_e}(\vec{J} \times \vec{B})\right],\qquad(1)$$

Where $\vec{J}$ is the electric current density vector, σ is the electric conductivity of the fluid, $\vec{v}$ is the velocity vector, $\vec{E}$ is the intensity vector of the electric field, $\vec{B}$ is the induced magnetic vector, e is the charge of an electron and n_e is the number density of electrons.

The fluid velocity vector is given by:

$$\vec{v}(y,t) = u(y,t)\vec{\imath} + v_0\vec{\jmath} + w(y,t)\vec{k},\qquad(2)$$

By neglecting the polarization effect, we get the electric field vector equal to zero ($\vec{E}=0$). The generalized Ohm's law equation (1) gives $J_y = 0$ everywhere in the flow. The current density components J_x and J_z are given as:

$$J_x = \frac{\sigma B_0}{1+m^2}(mu - w),\qquad(3a)$$

$$J_z = \frac{\sigma B_0}{1+m^2}(u + mw),\qquad(3b)$$

where, m is the Hall parameter, $m = \frac{\sigma B_0}{en_e}$.

The vector equation of motion for the fluid is governed by the momentum equation together with the generalized Ohm's law and non–Darcy's resistance and can be written as:

$$\rho\frac{D\vec{v}}{Dt} = -\nabla p + \nabla.(\mu\nabla\vec{v}) + \vec{J} \times \vec{B} - \frac{\mu}{K}\vec{v} - \frac{\lambda\rho}{K}|\vec{v}|\vec{v},\qquad(4)$$

where, ρ is the density of the fluid, D/Dt is a differential operator, t is the time, K is the Darcy permeability, λ is the inertial coefficient, and μ is the apparent viscosity.

The two components of the momentum equation (4) in the x and z-direction become:

$$\rho\frac{\partial u}{\partial t} + \rho v_0\frac{\partial u}{\partial y} = \frac{-\partial p}{\partial x} + \frac{\partial}{\partial y}\left(\mu\frac{\partial u}{\partial y}\right) - \frac{\sigma B_0^2}{1+m^2}(u + mw) - \frac{\mu}{K}u - \frac{\lambda\rho}{K}u^2$$

$$,\qquad(5)$$

$$\rho\frac{\partial w}{\partial t} + \rho v_0\frac{\partial w}{\partial y} = \frac{\partial}{\partial y}\left(\mu\frac{\partial w}{\partial y}\right) - \frac{\sigma B_0^2}{1+m^2}(w - mu) - \frac{\mu}{K}w - \frac{\lambda\rho}{K}w^2$$

$$,\qquad(6)$$

where, u and v are velocity components in the x- and z-directions.

The energy equation describing the temperature distribution for the fluid and Joule dissipations is given by Attia et al.[25]:

$$\rho c_p\frac{\partial T}{\partial t} + \rho c_p v_0\frac{\partial T}{\partial y} = k\frac{\partial^2 T}{\partial y^2} + \mu\left[\left(\frac{\partial u}{\partial y}\right)^2 + \left(\frac{\partial w}{\partial y}\right)^2\right] + \frac{\sigma B_0^2}{1+m^2}(u^2 + w^2)$$

$$(7)$$

where, c_p and k are the specific heat capacity and the thermal conductivity of the fluid, respectively and T denotes the temperature. The second and third terms on the right side represent, respectively, the viscous and Joule dissipations. We notice that each of these terms has two components. This is because the Hall effect leads to an additional velocity component w in the z-direction.

The shear stress τ of the Bingham fluid model can be written as follows[25]:

$$\begin{aligned}\tau &= \tau_0 + K_B\acute{\gamma} && for\ |\tau| > \tau_0\\ \acute{\gamma} &= 0 && for\ |\tau| \le \tau_0\end{aligned}$$

where, $\acute{\gamma} = \sqrt{\left(\frac{\partial u}{\partial y}\right)^2 + \left(\frac{\partial w}{\partial y}\right)^2}$ is the shear rate, τ_0 is the yield stress, K_B is the plastic viscosity of the Bingham fluid. Thus, the apparent viscosity is given by:

$$\mu = K_B + \frac{\tau_0}{|\acute{\gamma}|},\qquad(8)$$

Owing to provides no information about the stress field whenever $\tau < \tau_0$, and is discontinuous. In order to avoid this discontinuity, Papanastasiou [27] proposed a modified model with a growth rate parameter m which controls the exponential growth of stress. Thus the Bingham model can be re-written by using Papanastasiou modification as follows:

$$\tau = \tau_0[1 - e^{-\delta\acute{\gamma}}] + K_B\acute{\gamma}\qquad for\ all\ \acute{\gamma},\qquad(9)$$

The parameter m controls the stress growth, such that the yield stress τ_0 a finite stress is allowed to vanish, therefore this model is valid for all regions [28]. For sufficiently the parameter $\delta > 100$ in the above equation mimics the Bingham plastic model [28]. Thus, the scalar viscosity is given by:

$$\mu = K_B + \frac{\tau_0[1-e^{-\delta|\acute{\gamma}|}]}{|\acute{\gamma}|},\qquad(10)$$

The initial and boundary conditions of both the flow and heat problems are, respectively, given by:

$$At\ t \le 0: u = w = 0;\ T = T_1,\qquad(11a)$$
$$At\ t > 0: u = w = 0;\ T = T_1$$
$$at\ y = -h,\qquad(11b)$$
$$At\ \ t > 0: u = U_0;\ w = 0;\ T = T_2$$
$$at\ y = h.\qquad(11c)$$

The following non-dimensional variables will be introduced into equations (5)-(7) and (10)-(11):

$$x^* = \frac{x}{h}, y^* = \frac{y}{h}, z^* = \frac{z}{h}, t^* = \frac{tU_0}{h},$$
$$u^* = \frac{u}{U_0}, w^* = \frac{w}{U_0}, p^* = \frac{p}{\rho U_0^2},$$
$$T^* = \frac{T-T_1}{T_2-T_1}, \mu^* = \frac{\mu}{K_B}.$$

The non-dimensional conservation equations will be in the following forms:

Momentum conservation in the x-direction:

$$\frac{\partial u^*}{\partial t^*} + s\frac{\partial u^*}{\partial y^*} = \frac{-\partial p^*}{\partial x^*} + \frac{1}{R_e}\frac{\partial}{\partial y^*}\left(\mu^*\frac{\partial u^*}{\partial y^*}\right) - \frac{Ha^2}{R_e(1+m^2)}(u^* + mw^*) - \beta\mu^*u^* - \gamma u^{*2}$$

(12)

Momentum conservation in the z-direction:

$$\frac{\partial w^*}{\partial t^*} + s\frac{\partial w^*}{\partial y^*} = \frac{1}{R_e}\frac{\partial}{\partial y^*}\left(\mu^*\frac{\partial w^*}{\partial y^*}\right) - \frac{Ha^2}{R_e(1+m^2)}(w^* - mu^*) - \beta\mu^*w^* - \gamma w^{*2}$$

(13)

Energy conservation:

$$\frac{\partial T^*}{\partial t^*} + s\frac{\partial T^*}{\partial y^*} = \frac{1}{R_e P_r}\frac{\partial^2 T^*}{\partial y^{*2}} + \frac{E_c\mu^*}{R_e}\left[\left(\frac{\partial u^*}{\partial y^*}\right)^2 + \left(\frac{\partial w^*}{\partial y^*}\right)^2\right] + \frac{E_c Ha^2}{R_e(1+m^2)}(u^{*2} + w^{*2})$$

(14)

The apparent viscosity:

$$\mu^* = 1 + \frac{\tau_D\left[1 - e^{-\eta\sqrt{\left(\frac{\partial u^*}{\partial y^*}\right)^2 + \left(\frac{\partial w^*}{\partial y^*}\right)^2}}\right]}{\sqrt{\left(\frac{\partial u^*}{\partial y^*}\right)^2 + \left(\frac{\partial w^*}{\partial y^*}\right)^2}},$$

(15)

The dimensionless initial and boundary conditions of both the flow and heat problems are, respectively, given by:

At $t^* \leq 0: u^* = w^* = 0; T^* = 0$, (16a)

At $t^* > 0: u^* = w^* = 0; T^* = 0$

at $y = -1$, (16b)

At $t^* > 0: u^* = 1; w^* = 0; T^* = 1$

at $y = 1$, (16c)

where, $R_e = \frac{\rho U_0 h}{K_B}$ is the Reynolds number representing the ratio of inertial forces to viscous forces, $Ha^2 = \frac{\sigma B_0^2 h^2}{K_B}$ is the Hartmann number squared which represents the ratio of electromagnetic force to the viscous force, $P_r = \frac{\mu c_p}{k}$ is the Prandtl number which dimensionless number defines the ratio of the momentum diffusivity (kinematic viscosity) to thermal diffusivity, $\tau_D = \frac{\tau_0 h}{K_B U_0}$ is the dimensionless yield stress, $S = \frac{v_0}{U_0}$ is the suction parameter representing the mass of the fluid passing through the lower plate and exiting through the upper plate (when $S > 0$ the suction at the upper plate and injection at the lower plate), $E_c = \frac{U_0^2}{c_p(T_2-T_1)}$ is the Eckert number which defines the ratio of the kinetic energy of the flow to the enthalpy difference, $\beta = \frac{h^2}{R_e K}$ is the porosity parameter, $\gamma = \frac{\lambda h}{K}$ is the dimensionless non-Darcy parameter, and $\eta = \frac{\delta U_0}{h}$ is the dimensionless growth parameter.

NUMERICAL SOLUTION

There are many numerous methods available for the solution of the differential equation system. In the present work the finite difference method is used to solve the coupled non-linear partial differential equation systems (12)–(15) under conditions (16a), (16-b), and (16-c). The computational domain is discretized with a uniform grid of dimension Δt and Δy in time and space respectively as shown in Figure 2. A finite difference scheme for coupled partial differential equation systems (12)–(15) is created using the Crank-Nicolson implicit method which can be achieved by doing an average of the central difference schemes at time levels n and n+1.

To solve for the n+1th time step, where we know already the nth time step, we consider our scheme as if we were standing at the n +0.5 time step and then take the average of the forward half time step and backward half time step. So the discretized equations would be of the form:

x-direction momentum equation:

$$\frac{u_i^{*n+1} - u_i^{*n}}{\Delta t} + s\left(\frac{u_{i+1}^{*n+1} - u_{i-1}^{*n+1} + u_{i+1}^{*n} - u_{i-1}^{*n}}{4\Delta y}\right) = -C + \frac{1}{R_e}\left(\frac{\mu_{i+1}^{*n+1} - \mu_{i-1}^{*n+1} + \mu_{i+1}^{*n} - \mu_{i-1}^{*n}}{4\Delta y}\right)\left(\frac{u_{i+1}^{*n+1} - u_{i-1}^{*n+1} + u_{i+1}^{*n} - u_{i-1}^{*n}}{4\Delta y}\right) + \frac{1}{R_e}\left(\frac{\mu_i^{*n+1} + \mu_i^{*n}}{2}\right)\left(\frac{u_{i+1}^{*n+1} - 2u_i^{*n+1} + u_{i-1}^{*n+1}}{2\Delta y^2} + \frac{u_{i+1}^{*n} - 2u_i^{*n} + u_{i-1}^{*n}}{2\Delta y^2}\right) - \frac{Ha^2}{R_e(1+m^2)}\left(\frac{u_i^{*n+1} + u_i^{*n}}{2} + m\frac{w_i^{*n+1} + w_i^{*n}}{2}\right) - \beta\left(\frac{\mu_i^{*n+1} + \mu_i^{*n}}{2}\right)\left(\frac{u_i^{*n+1} + u_i^{*n}}{2}\right) - \gamma\left(\frac{u_i^{*n+1} + u_i^{*n}}{2}\right)^2$$

(17)

y-direction momentum equation:

$$\frac{w_i^{*n+1} - w_i^{*n}}{\Delta t} + s\left(\frac{w_{i+1}^{*n+1} - w_{i-1}^{*n+1} + w_{i+1}^{*n} - w_{i-1}^{*n}}{4\Delta y}\right) = \frac{1}{R_e}\left(\frac{\mu_{i+1}^{*n+1} - \mu_{i-1}^{*n+1} + \mu_{i+1}^{*n} - \mu_{i-1}^{*n}}{4\Delta y}\right)\left(\frac{w_{i+1}^{*n+1} - w_{i-1}^{*n+1} + w_{i+1}^{*n} - w_{i-1}^{*n}}{4\Delta y}\right) + \frac{1}{R_e}\left(\frac{\mu_i^{*n+1} + \mu_i^{*n}}{2}\right)\left(\frac{w_{i+1}^{*n+1} - 2w_i^{*n+1} + w_{i-1}^{*n+1}}{2\Delta y^2} + \frac{w_{i+1}^{*n} - 2w_i^{*n} + w_{i-1}^{*n}}{2\Delta y^2}\right) - \frac{Ha^2}{R_e(1+m^2)}\left(\frac{w_i^{*n+1} + w_i^{*n}}{2} - m\frac{u_i^{*n+1} + u_i^{*n}}{2}\right) - \beta\left(\frac{\mu_i^{*n+1} + \mu_i^{*n}}{2}\right)\left(\frac{w_i^{*n+1} + w_i^{*n}}{2}\right) - \gamma\left(\frac{w_i^{*n+1} + w_i^{*n}}{2}\right)^2$$
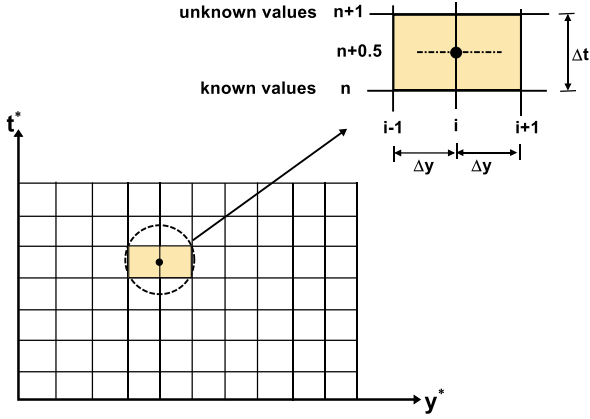
, (18)

Fig. 2. Mesh layout for the Crank-Nicolson implicit method.

Similarly, the Crank-Nicolson approximation to the Energy equation is:

$$\frac{T^{*n+1}_i - T^{*n}_i}{\Delta t} + s\left(\frac{T^{*n+1}_{i+1} - T^{*n+1}_{i-1} + T^{*n}_{i+1} - T^{*n}_{i-1}}{4\Delta y}\right) =$$
$$\frac{1}{P_r R_\varepsilon}\left(\frac{T^{*n+1}_{i+1} - 2T^{*n+1}_i + T^{*n+1}_{i-1}}{2\Delta y^2} + \frac{T^{*n}_{i+1} - T^{*n}_i + T^{*n}_{i-1}}{2\Delta y^2}\right) +$$
$$\frac{E_c}{R_\varepsilon}\left(\frac{\mu^{*\,n+1}_i + \mu^{*\,n}_i}{2}\right)\left(\left(\frac{u^{*n+1}_{i+1} - u^{*n+1}_{i-1} + u^{*n}_{i+1} - u^{*n}_{i-1}}{4\Delta y}\right)^2 +\right.$$
$$\left(\frac{w^{*n+1}_{i+1} - w^{*n+1}_{i-1} + w^{*n}_{i+1} - w^{*n}_{i-1}}{4\Delta y}\right)^2\right) +$$
$$\frac{E_c Ha^2}{R_\varepsilon(1+m^2)}\left(\left(\frac{u^{*n+1}_i + u^{*n}_i}{2}\right)^2 + \left(\frac{w^{*n+1}_i + w^{*n}_i}{2}\right)^2\right)$$

, (19

Finally, the resulting block tri-diagonal system is solved using the generalized Thomas-algorithm. All calculations are carried out for the non-dimensional variables and parameters given by, $\frac{\partial p^*}{\partial x^*} = C = -5$. Grid-independence studies show that the computational domain $0 < t < \infty$ and $1 < y < 1$ is divided into intervals with step sizes $\Delta t = 0.0001$ and $\Delta y = 0.005$ for time and space respectively.

RESULTS AND DISCUSSION

Figures 3-5 show the evolution of dimensionless velocities u^* and w^* and temperature distribution T^* with time t^* for various Darcy and non-Darcy parameters (β and γ) at *Ha=3, m=3, S=1, R_e=10, P_r=1, E_c=0.2* and $\tau_D = 0.1$. Figures 3 and 4 show the effect of Darcy and non-Darcy parameters (β and γ) on the time development of u^* and w^*. It is obvious that increasing the Darcy parameter β decreases u^* and w^* and its steady state time as a result of increasing the resistive damping porosity force on u^* and w^*. On the other hand, increasing the non- Darcy parameter γ for each value of β decreases the velocity u^* and w^* and its steady state

time which reflects the expected resistance because of the inertial effects.

Also, it is observed that the charts of the velocity u^* are asymmetric about the $y = 0$ plane because of the suction. Figure 5 shows the effect of Darcy and non- Darcy parameters on the time progression of the temperature T^*. It is observed that the increase of the Darcy parameter β and non-Darcy parameter γ decreases T^* and its steady state time. The increasing β and γ decreases u^* which in turn decreases the viscous dissipation and T^*. Also, increasing the non- Darcy parameter γ for each value of β further decreases the temperature and its steady time because of the additional resistive inertial effects. Figures 3-a, 4-a, and 5-a, indicate the unsteady non-Newtonian Bingham fluid case where the plates and medium are non-porous ($\beta=0$ and $\gamma=0$) obtaining the highest velocity and temperature distributions, which were considered earlier by Attia [25].In addition, we mean a flow without additional inertial effects and the Darcy case where $\beta=1$ and $\gamma=0$ as shown in figures 3-b, 4-b and 5-b, obtained to provide an easier quick path for the fluid flow and temperature values.
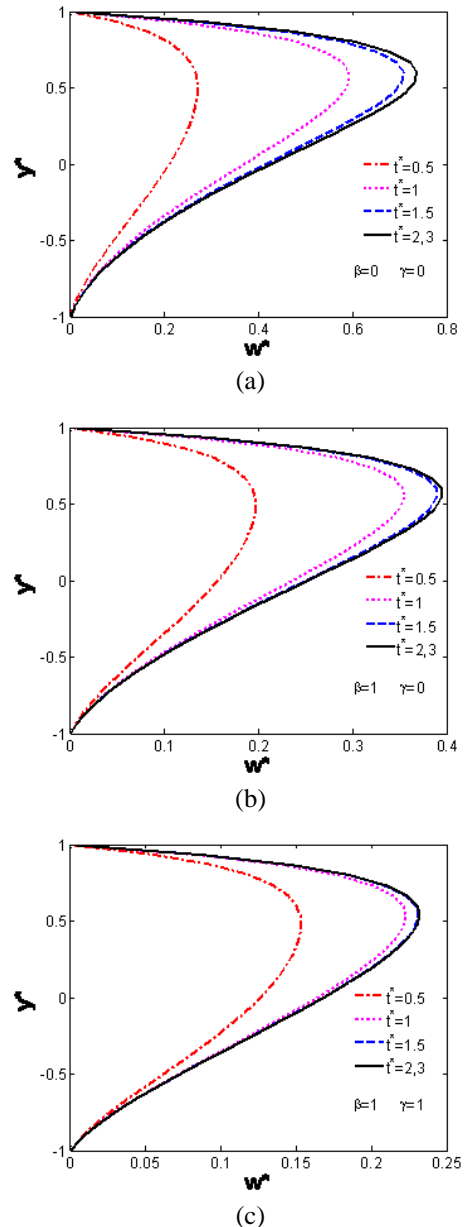
Figure 6 presents the profiles of the velocity component u^* and w^* and temperature distribution T^* at the center of the channel ($y^* = 0$) with time t^* for various non-Darcy parameters γ and for $\tau_D = 0.01\ and\ 0.1$ at *Ha=3, m=3, S=1, R_e=10, P_r=1,E_c=0.2*. The figures show that, with increasing the yield stress τ_D decreases the velocity components u^* and w^* and temperature profile T^*, the time at which they reach their steady state values also decreases as a result of increasing the viscosity. It is obvious that increasing the non-Darcy parameter γ decreases u^*, w^*, T^* and its steady state time as a result of increasing the resistive damping porosity force on u^* and w^*. Also, it observed that the velocity component u^* reaches the steady state faster than w^* which, in turn, reaches the steady state faster than T^*. This is expected as u^* is the source of w^*, while both u^* and w^* act as sources for the temperature.

The influence of the non-Darcy parameter γ on the velocity components u^*, w^* and temperature distribution T^* with time t^* for various Hartmann numbers Ha are shown in figure7 at the center of the channel ($y^* = 0$). It is clear that, with increasing the value of the non-Darcy parameter γ ($\gamma = 0,1,2$), there is a marked decrease in the velocity components u^* and w^*, i.e. the flow is accelerated strongly with the decrease in the non-Darcy parameter, owing to a simultaneous increase in the inertial force in equation (12) $-\gamma u^{*2}$ and in equation (13) $-\gamma w^{*2}$.

(a)

(b)

(c)
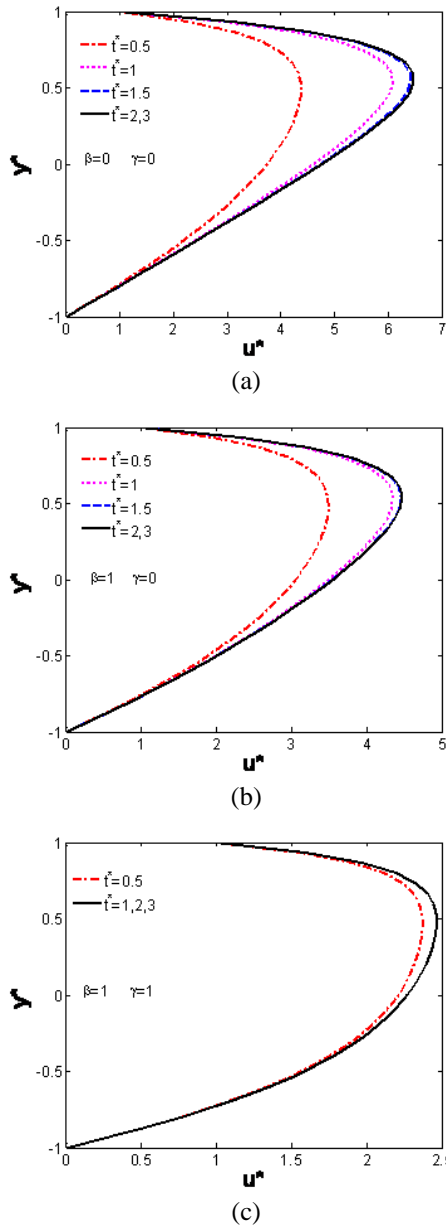
Fig. 3. Time variation of the profile of u^* for various values of γ and β. (a) $\beta=0$ and $\gamma=0$; (b) $\beta=1$ and $\gamma=0$; (c) $\beta=1$ and $\gamma=1$.
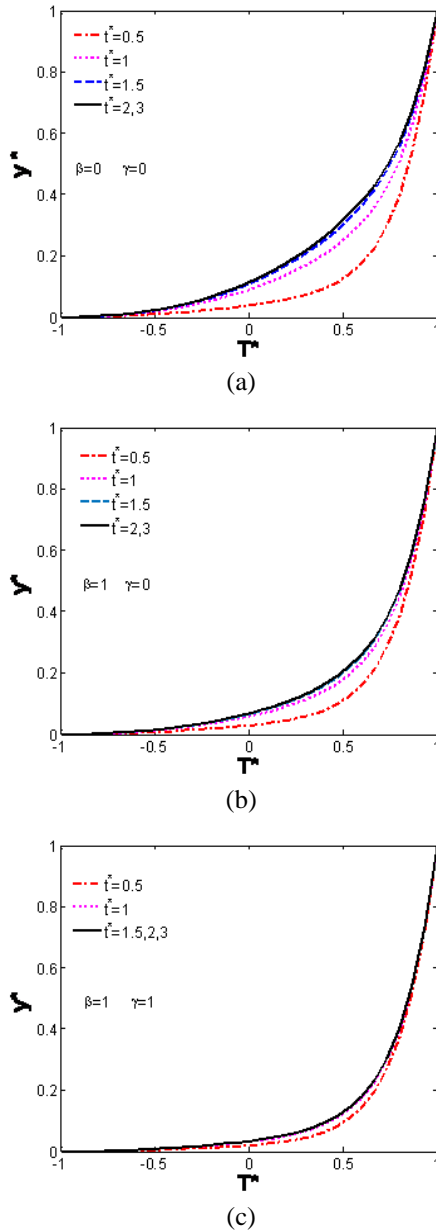

(a)

(b)

(c)

Fig. 4. Time variation of the profile of w^* for various values of γ and β. (a) $\beta=0$ and $\gamma=0$; (b) $\beta=1$ and $\gamma=0$; (c) $\beta=1$ and $\gamma=1$.

Figure 7-a shows that, with an increase of the Hartmann number Ha, the magnitude of the velocity component u^* is reduced because the hydromagnetic drag force in equation (12), $\frac{-Ha^2}{R_e(1+m^2)}(u^* + mw^*)$ is proportional to the square of Ha and remains with a negative sign. Therefore, by increasing the Hartmann number Ha creates a larger negative force. On the other hand, figure 7-b indicates the increase in the velocity component w^* with a rise in the Hartmann number because the hydromagneticforce in (13) $(\frac{-Ha^2}{R_e(1+m^2)}(w^* - mu^*))$ has two components, positive

$u^*(\frac{Ha^2}{R_e(1+m^2)}mu^*)$ and negative $w^*\left(\frac{-Ha^2}{R_e(1+m^2)}w^*\right)$, so the collective effect is markedly boosted with a rise in the Hartmann number. The temperature T^* is also increasing substantially with increasing the Hartmann number Ha indicating that the regime is cooled by stronger magnetic fields.

Figure 8 presents the influence of the non-Darcy parameter γ on the velocity components u^*, w^* and the temperature distribution T^* with time t^* for the Hall parameter m at $\beta =1$, $S=1$, $Ha=3$, $R_e=10$, $P_r=1$, $E_c=0.2$, $\tau_D=0.1$. It is clear that by increasing the non-Darcy parameter γ (inertial effect), u^*, w^* and T^* decrease.Figure 8-a, indicates that the velocity ofcomponent u^* increases by increasing the Hall

parameter m which can be attributed to the fact that an increment in m decreases the resistive force. Figure 8-b shows that the velocity component $w^{\bullet}$ decreases with the increasing Hall parameter *m* which can be attributed to the fact that an increment in *m* increases the resistive force. Figure 8-c shows that $T^{\bullet}$ decreases with the increasing Hall parameter *m* for all values of time as a result of an increase in the Hall current parameter m, will decrease the contribution from the Joule dissipation term.
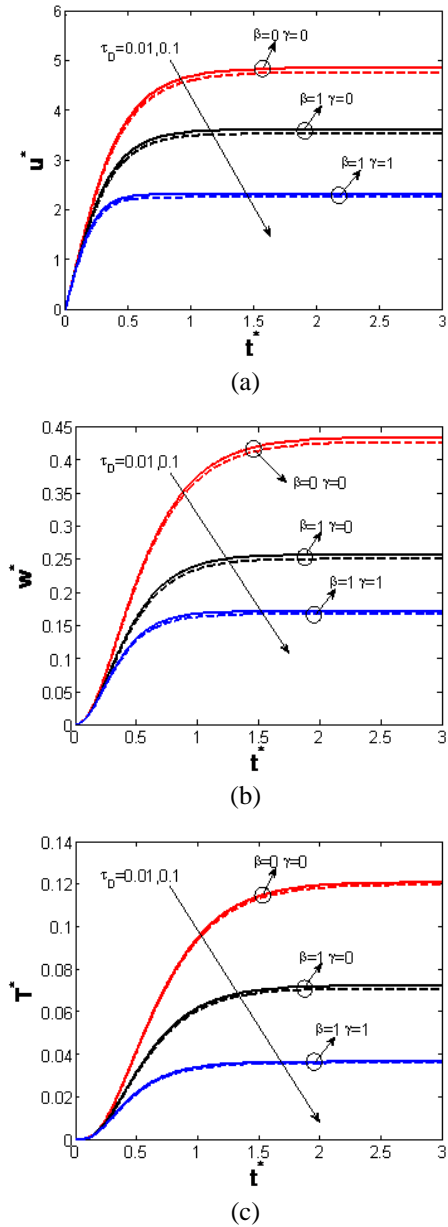

(a)

(b)

(c)

Fig. 5. Time variation of the profile of $T^{\bullet}$ for various values of γ and β. (a) *β=0* and *γ=0*; (b) *β=1* and *γ=0*; (c) *β=1* and *γ=1*.

CONCLUSIONS

The unsteady couette flow of non-Newtonian Bingham fluid between two parallel porous plates containing a non-Darcy porous medium has been

studied with heat transfer and the Hall effect in the presence of uniform suction and injection.

(a)

(b)

(c)

Fig. 6. $u^{\bullet}$, $w^{\bullet}$, and $T^{\bullet}$ versus $t^{\bullet}$ at cannel center ($y^{\bullet} = 0$) for various values of γ and β andvarious values τ_{D}. (a) $u^{\bullet}$; (b) $w^{\bullet}$; (c) $T^{\bullet}$ Profile.

The governing momentum and energy equations are solved numerically using the finite difference approximations. Through the numerical results the following can be concluded:

- The effects of the resistive porosity force and the inertial force (Darcy and non-Darcy parameters β and γ) on the velocity components and temperature distribution have been investigated. The increase in β and γ will decrease the velocity and temperature.
- The yield stress τ_{D} has a remarkable effect on the velocity components and temperature distribution. An increase occurred in τ_{D}

503

accompanied by a decrease in the velocity and temperature as well as their steady state time.

- The effects of the Hartmann number *Ha* on the velocity components and temperature distribution have been studied. By increasing *Ha* the x-component of the velocity will decrease, while the z-component of the velocity and temperature will increase.

- The effect of the Hall parameter *m* on the velocity components and temperature distributions has been assessed. The Hall parameter *m* is directly proportional to the x-component of the velocity while it is inversely proportional to the z-component of the velocity and temperature distribution.
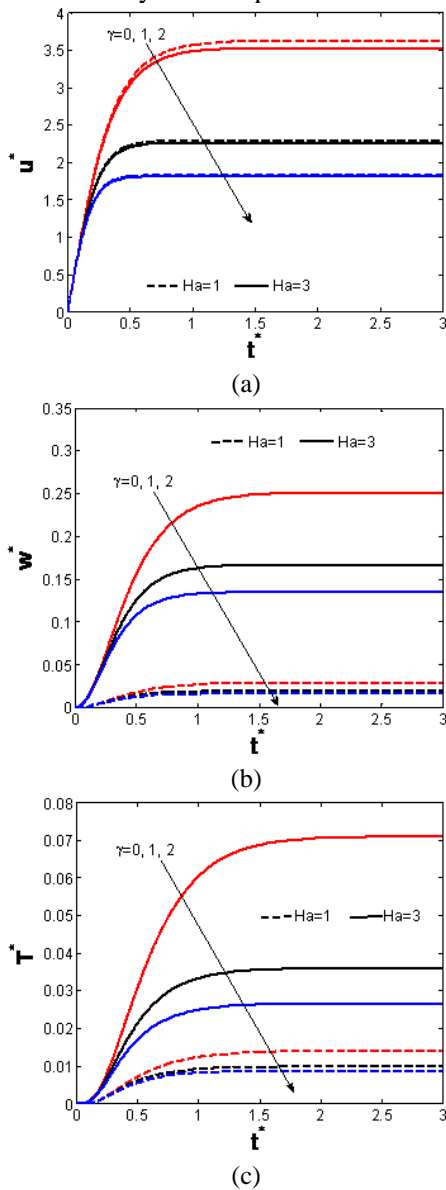

(a)

(b)

(c)

Fig. 7. Effect of the non-Darcian parameter γ on u^*, w^*, and T^* profiles at the cannel center for low and high Hartmann number *Ha*. (a) u^*; (b) w^*; (c) T^* Profile
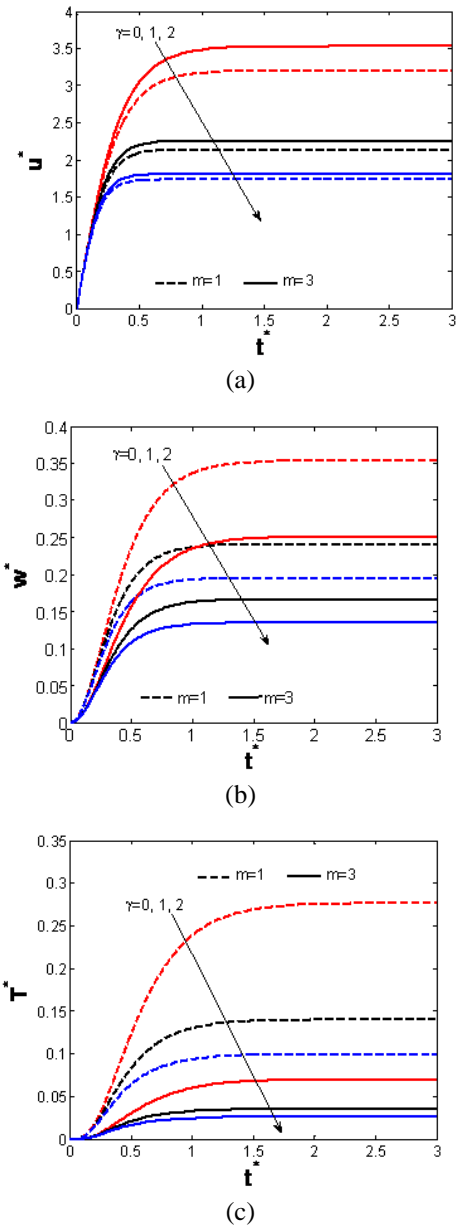

(a)

(b)

(c)

Fig. 8. Effect of the non-Darcian parameter γ on u^*, w^*, and T^* profiles at cannel center for various values of the Hall parameter *m*. (a) u^*; (b) w^*; (c) T^* Profile

REFERENCES

1. B. Devika, P. V. Narayana, S. Venkataramana, *International Journal of Engineering Science Invention,* **2**, 26(2013).
2. H. A. Attia, W. Abd El-Meged , W. Abbas, M. A. M. Abdeen, *International Journal of Civil Engineering,* **12**, 277 (2014).
3. A. Bharali and A. K. Borkakati,*Applied Scientific Research*, **39**, 155 (1982).
4. H. A. Attia, N. A. Kotb, *Actamechanica*, **117**, 215 (1996).
5. Z. Joaquín, E. Pablo, G. Enrique, L. M. José, A. B. Osman, *Int. Comm. Heat and Mass Trans.*, **37**, 1432 (2010).
6. H. A. Attia, W. Abbas, M. A. M. Abdeen, A. E.-D. Abdin, *Blug. Chem. Commun.*, **46**, 535 (2014).

7. E. Sweet, K. Vajravelu, R. A. Van Gorder, I. Pop, *Commun Nonlinear SciNumerSimulat*, **16**, 266 (2011).

8. H. A. Attia, W. Abbas, M. A. M. Abdeen, M. S. Emam, *European Journal of Environmental and Civil Engineering*, **18**, 241 (2014).

9. H. A. Attia, W. Abbas, M. A. M. Abdeen, A. A. M. Said, *Sadhana*, **40**(1), 183 (2015).

10. H. A. Attia, W. Abbas, A. El-Din Abdin, M. A. M. Abdeen, High Temperature, **53**, 891 (2015).

11. C-C. Liu, C-Y. Lo, *International Communications in Heat and Mass Transfer*, **39**, 1354 (2012).

12. H. A. Attia, W. Abbas, M. A. M. Abdeen, *Journal of the Brazilian Society of Mechanical Sciences and Engineering,* in press, Available online 11 February, 2015.

13. I. C. Walton, S. H. Bittleston, *J. Fluid Mech.*, **222**, 39 (1991).

14. S.Yang, K. Zhu, *J. Non-Newtonian Fluid Mech.*, **138**, 73 (2006).

15. D. A. S. Rees , A. P. Bassom, *International Journal of Heat and Mass Transfer* , **82**, 460 (2015).

16. Z. Zeng, R. Grigg, *Transport In Porous Media*, **63**, 57 (2006).

17. O.A. Bég, J. Zueco, H.S. Takhar, *Communications in Nonlinear Science and Numerical Simulation*, 14, 1082 (2009).

18. A. Matthew, M. Sc. Thesis, Texas Tech University, Lubbock, Texas, United States, 2006.

19. Y. J. Kim, *International Journal of Engineering sciences*, **38**, 833 (2000).

20. D. Pal, B. Talukdar, *International Journal of Appl. Math. and Mech.*, **7**, 58 (2011).

21. S. S. Das, M. Maity, J. K. Das, *International Journal of Energy and Environment*, **1**, 109 (2012).

22. A.A. Moniem, W. S. Hassanin, *Applied Mathematics*, **4**, 694 (2013).

23. A. Afify, *Transport in Porous Media*, **66**, 391 (2007).

24. O. A. Bég, J. Zueco, R. Bhargava, H. S. Takhar, *International Journal of Thermal Sciences*, **48** , 913 (2009).

25. H. A. Attia, M E. Sayed-Ahmed, *Applied Mathematical Modelling,* **28**, 1027 (2004).

26. Abdeen M. A. M, Attia H A, Abbas W, Abd El-Meged W, *Indian Journal of Physics*, **87**, 767 (2013).

27. T. C. Papanastasiou, *J. Rheol.*, **31**, 385 (1987).

28. E. Mitsoulis, *The British Society of Rheology*, **135**, 135 (2007).

ОТКЛОНЕНИЯ ОТ ЗАКОНА НА ДАРСИ ПРИ НЕНЮТОНОВИ БИНГАМОВИ ФЛУИДА С ТОПЛОПРЕНАСЯНЕ МЕЖДУ ДВЕ УСПОРЕДНИ ПЛОСКОСТИ

У. Аббас[1], Х. Али Атия[2], М.А.М. Абдийн[3]

[1]*Департамент по основни и приложни науки, Колеж по инженерство и технологии, Арабска академия за наука, технологии и морски транспорт, Кайро, Египет*

[2]*Департамент по инженерство, математика и физика, Инженерен факултет, Университет Ел-Фаюм, Ел-Фаюм - 63514, Египет*

[3]*Департамент по инженерство, математика и физика, Инженерен факултет, Университет в Кайро, Гиза-12211, Египет*

(Резюме)

Моделът на не-Дарси'ев поток за Бингамови флуиди има широк кръг от приложения в енергийните системи и обработката на магнитни материали. Тази работа изследва ефекта на не-Дарси'ево течение върху разпределението на скоросиютите и температурата за не-нютонов Бингамов флуид между две безкрайни успоредни порьозни плоскости с топлопренасяне отчитайки ефекта на Хол. По главното надлъжно направление се прилага постоянен градиент на налягането, перпендикулярно на плоскостите се прилага постоянно външно магнитно поле, както и равномерно всмукване и впръскване.в същото направление. Изведение са и числено са решени безизмерните уравнения на движението и енергията, отчитащи механичната и вискозната дисипация на енергията. Иследвани са ефектите на порьозността на средата, на Хартман и Хол, на скоростта и разпределението на температурата за число на Рейнолдс равно на 10 (за $Re_e \geq 10$ не-Дарсие'вият модел е достатъчен). Намерено е, че порьозността и инерционните ефекти имат забележимо влияние върху разпределението на скоростите. Освен това, нарастването на не-Дарси'евия параметър понижава температурата при всяка порьозност.